

## OPTIMIZATION ANALYSIS ON THE SUPPORT PERFORMANCE OF COMPOSED ANCHOR ROD COMPONENTS IN GOB-SIDE ROADWAY

Jiang YU<sup>1,2</sup>, Linlin JIN<sup>2</sup>, Hongfa MA<sup>2\*</sup>,  
Jun ZHANG<sup>1</sup>, Feng WANG<sup>1,2</sup>, Xin HE<sup>1</sup>, Dawei YIN<sup>2</sup>

<sup>1</sup> Shandong Energy Group Northwest Mining Co., Ltd, Xi'an, Shanxi, 710018, China

<sup>2</sup> Shandong University of Science and Technology, Qingdao, Shandong, 266590, China

---

**Abstract:** In response to the failure problem of the roadway support structure for the deep buried mine, the mechanical calculation model was established based on the stress state and the boundary conditions of the composed anchor rod under the large surrounding rock deformation, and the failure discrimination criterion was obtained. Then a structural analysis unit for rock-composed anchor was established using ANSYS simulation software, which intensively researched the single-point and local failure characteristics of anchor rods in gob-side entries, and the optimization measures of the composed anchor rods were proposed. The findings reveal that the higher preload could restrain the axial displacement of the anchor rod, leading to stress concentration, fracture, or loosening of anchor bolts or nuts by the insufficient rock deformation. In addition, the stress concentration and plastic deformation of pallet orifice are significant as the main pressure-bearing part. The increase in the surrounding rock deformation leads to an enhanced combined action of pressure and shear force between the steel strip and the pallet edge, which makes the steel strip prone to failure. Consequently, the optimization measures of reducing prestress and increasing the size of pallet and strip are proposed, which can effectively control the deformation of surrounding rock and reduce the stress concentration, plastic deformation and failure rate of composed anchor rod.

---

**Keywords:** *gob-side entry, composed anchor rods, ANSYS, support performance*

---

\* Corresponding author: mh930412@163.com (H. Ma)

## 1. INTRODUCTION

Anchor rods have become the most widely used supporting method to maintain roadway stability due to their strong adaptability (Lubryka et al. 2023). In addition, the anchor rod structure has a developing process from ordinary anchor rods to composed anchor rods, and the support performance of composed anchor rods is higher than that of ordinary anchor rods, with a support rate of 90%, which is superior in controlling surrounding rock deformation (Jing et al. 2022; Zhang et al. 2012; Shi et al. 2024). In order to improve coal mining rate and alleviate the mining tension, the mining technology of gob-side entry is continuously promoted. However, the engineering practice has shown that there are obvious underground pressure and surrounding rock deformation in the gob-side entries (Wu et al. 2025; Wang et al. 2025), which might also be an important reason for the failure of anchor rods (Zeqiri et al. 2021; Sakhno et al. 2021; Bondarenko et al. 2018; Ming et al. 2023). Therefore, a large number of scholars have conducted extensive research on the failure mechanism of anchor rods and the supporting structures optimization in gob-side entries.

Mesutoglu et al. (2024) explored the feasibility of anchor rod support in thick coal seam underground coal mine tunnels through on-site research and indoor experiments. Cao et al. (2020) and Wang et al. (2023) studied the ultimate support effect of pre-stressed anchor bolts and the plastic deformation behavior, and proposing a super anchor support scheme based on high pre-stress support technology. Zhou et al. (2023) used the ANSYS simulation software to establish a model of iron-wood composed pallet, and studying the support mechanism and advantages of iron-wood composed pallets. Liu et al. (2020) and Zhang et al. (2022) analyzed the failure mechanism of anchor rod support under high ground stress based on the elastic-plastic solution of deep buried roadways and the neutral point theory of anchor rods, and studied the yield characteristics of different support components of the anchor rod breakage. Khademian et al. (2024) used the UDEC simulation software to study the mechanism of roof failure in longwall tunnels, and explored the influence of anchor cables, anchor rod density and strip support on roof instability. Tan et al. (2019) proposed a method for determining the parameters of the fixed support structure along the gob by establishing a roof support composed structure model, and studied the collaborative bearing characteristics of goaf and roof support. Xie et al. (2024) proposed the external anchor internal unloading collaborative control technology by analyzing the main causes of surrounding rock deformation of the gob-side entry. Wang et al. (2018) studied the preload effect on the strength of anchor rod support by analyzing the stress distribution of surrounding rock under different preload, and the results showed that reducing the preload appropriately had no significant impact on the surrounding rock. Zhao et al. (2023) and Zha et al. (2018) conducted simulation experiments on anchored rock masses using FLAC, studied the relationship between the surrounding rock of the tunnel and the support parameters of the deep roadway, and analyzed the effects of preload force and support spacing on

the surrounding rock stability by using the combined arch theory. Rong et al. (2021) established a numerical simulation model of the roadway anchor support system, proposed the evaluation of anchor support effect and optimization parameters, and established a mine pressure monitoring scheme. Wu et al. (2019) conducted the numerical simulations of drop weight impact tests on the end-anchored rock bolt using finite element method, and studied the influence of radial stiffness of surrounding rock on the dynamic characteristics of the end-anchored rock bolt.

The above research results have guiding significance for the failure of surrounding rock support components in gob-side entries. However, the failure mechanism of the composed anchor remains unclear, which severely limits the effective control of surrounding rock in gob-side entries and efficient production in mines. In this study, the ANSYS numerical simulation software was used to establish a structural analysis unit for rock-composed anchor rods. Based on the stress state of each component, the corresponding mechanical models were established to obtain the failure discrimination conditions of composed anchor rod components. Based on the single point and local failure characteristics of composed anchor, the support optimization measures to reduce the failure rate of the composed anchor were proposed to control the surrounding rock deformation effectively.

## 2. ANALYSIS OF THE STRESS STATE OF COMPOSED ANCHOR

Based on the stress state and boundary conditions of the composed anchor rod, the mechanical models were constructed (Fig. 1). Because the anchor rod length is much larger than the cross-sectional, the anchor is treated as a rod in material mechanics during the analysis (Si et al. 2022). The mechanical parameters are as follows.

(1) Anchor rod failure calculation (Kang et al. 2015):

$$\begin{cases} \tau = \frac{16M_t}{\pi d^3} \\ \sigma_{\max} = \frac{\sqrt{[32F_1(L - L_1) + 4dF]^2 + 768M_t^2}}{\pi d^3} \end{cases}, \tag{1}$$

where  $\tau$  is the maximum shear stress,  $\sigma_{\max}$  is maximum composed stress,  $F_1$  is the concentrated force at the tail of the anchor rod,  $F$  is the axial force on the anchor rod,  $d$  is the anchor rod diameter,  $L$  is distance from the fixed end of the anchor rod to the point of concentrated force application,  $L_1$  is distance from the fixed end of the anchor rod to the hole opening,  $M_t$  is nut torque, 300 N·m.

(2) Nut failure calculation (Liu et al. 2019):

$$\begin{cases} F_f = Tf \\ T = [8kM_t(1 - \alpha^3)] / [3DI(-\alpha^4)f], k = 0.5, \\ \alpha = d / D \end{cases} \quad (2)$$

where  $F_f$  is the frictional force on the nut,  $f$  is the coefficient of friction, 0.14,  $T$  is the preload force,  $M_t$  is the preload torque,  $d$  is the inner diameter of the nut,  $D$  is the outer diameter of the nut.

(3) Pallet failure calculation (Pan et al. 2023):

$$P = 2\sigma_s \pi b \frac{hr^2}{h^2 + r^2}, \quad (3)$$

where  $P$  is the load applied by the anchor rod to the pallet through the end nut,  $\sigma_s$  is the pallet yield stress,  $b$  is the pallet thickness,  $r$  is the circumference radius of the bottom surface of the arch,  $h$  is the arch height.

(4) Calculation of steel strip failure:

$$F \geq F_s, \quad (4)$$

where  $F$  is the shear stress on the steel strip,  $F_s$  is the shear strength of the steel strip.

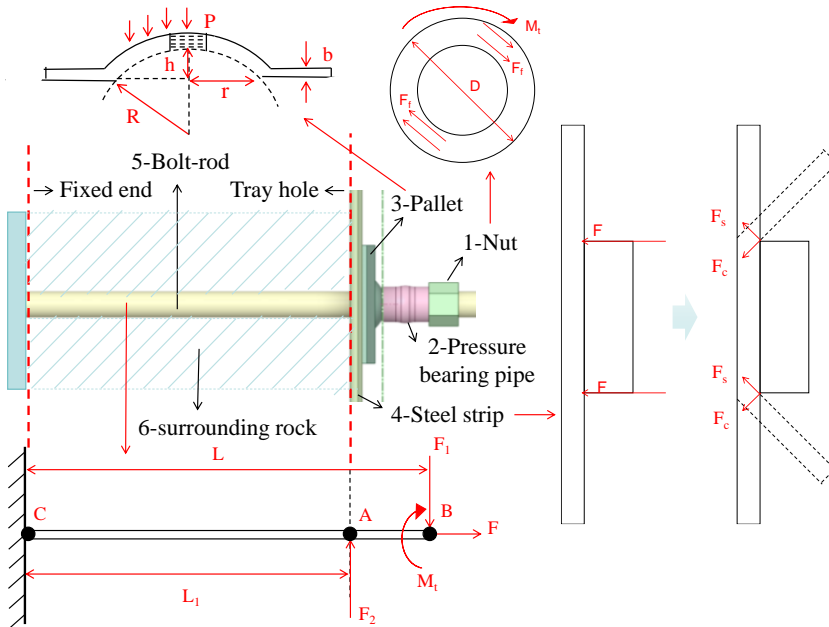


Fig. 1 Mechanical model of composed anchor rod

In summary, when the preload is 100 kN, the concentrated force  $F_1$  on the anchor rod is 3.33 kN, so the rod end would break when the shearing force of rod is  $F_1 \geq 3.33$  kN. Identically, the maximum friction force  $F$  of the nut is 68.6 kN, so the nut would fall off when the external force is  $F \geq F_f$ . Moreover, the pallet would fail when the maximum bearing capacity of the pallet is 325 MPa, and the steel strip would fracture when the shear stress on the steel strip exceeds 483 MPa at the same time. The composed anchor rods have a strong overall support effect, but the supporting components failure would lead to a decrease in the support effect of the composed anchor rod (Wu et al. 2020). Therefore, the geometric and mechanical parameters of anchor rods should be matched to ensure the overall support effect of the support system (Wu et al. 2020).

### 3. SIMULATION ANALYSIS OF ANCHOR RODS SUPPORT

#### 3.1. SINGLE ANCHOR ROD SUPPORT

##### 3.1.1. ESTABLISHMENT OF NUMERICAL MODEL

To investigate the failure characteristics of composed anchor rods, the structural analysis unit of rock-composed anchor rod was established using Spaceclaim and ANSYS Workbench simulation software (Fig. 2). The surrounding rock model is the cube with a side length of 3 m, much larger than the anchor rod diameter, avoiding other factors that might affect the force on the anchor rod. Then, the displacement constraints are set at the model bottom, and the binding contacts are established between the surrounding rock and the anchor rod. The anchor rod size is  $\varnothing 22 \times 2800$  mm, with the yield strength of 500 MPa, the steel strip size is  $2200 \times 180 \times 5$  mm, with the yield strength of 355 MPa, the pallet size is  $100 \times 100 \times 10$  mm, and the arch height is 20 mm, with the yield strength of 235 MPa.

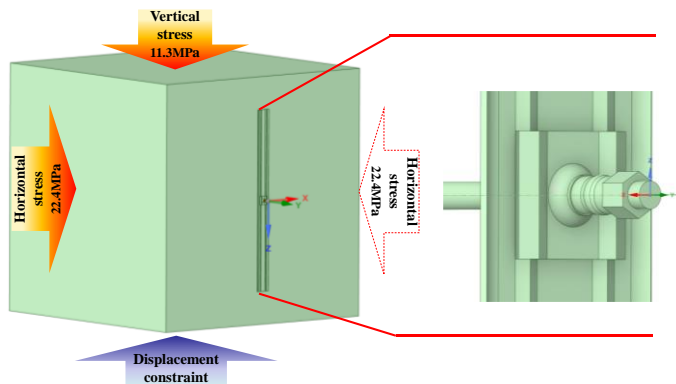


Fig. 2. Numerical model of single anchor rod

Table 1. Mechanical parameters of numerical models

Component name	Elastic modulus [GPa]	Density [kg·m <sup>-3</sup> ]	Poisson's ratio	Yield strength [MPa]
Surrounding rock	0.6	1350	0.25	16
Anchor rod	210	7800	0.3	500
Pallet	200	7800	0.3	235
Steel strip	206	7800	0.3	355

The mechanical parameters of the composed anchor rod are presented in Table 1. The preload is set to 100 kN, which is 52% of the rod yield force and comply with the *Chinese Standard: Technical Specifications for Rock Bolting in Coal Mine Roadways*. A reaction force equal to the preload but with a different direction is applied beneath the nut. According to the stress testing report, the horizontal stress and vertical stress of the surrounding rock are 22.4 MPa and 11.3 MPa, respectively.

3.1.2. THE FAILURE MODE OF ANCHOR ROD-NUT

Figure 3 shows the deformation characteristics of the nut-anchor rod, including the relative displacement curves. In Figure 3a, the tensile deformation at the rod end and

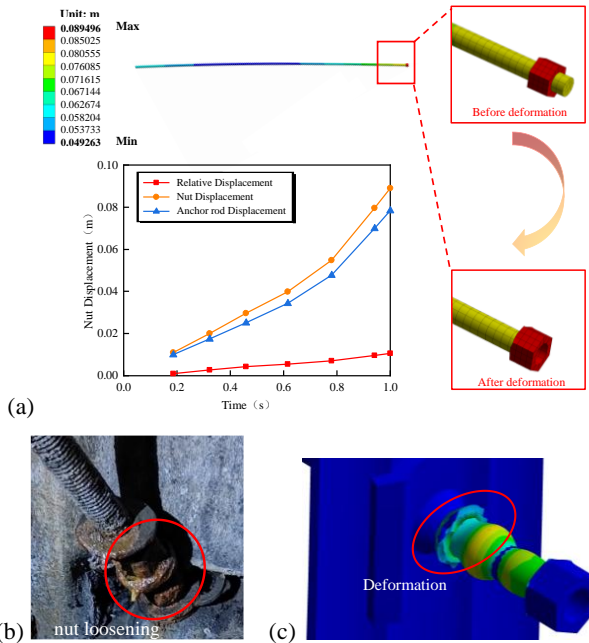


Fig. 3. The deformation characteristics of the nut-anchor rod: (a) nut-anchor rod deformation results, (b) diagram of onsite nut damage, (c) nut deformation cloud map

the relative displacement between the nut and anchor rod gradually increase with the surrounding rock deformation increasing. As a consequence, when the force on the nut end exceeds the frictional force provided by the thread, the nut would fall off. Moreover, Figures 3b and 3c show the bending deformation in the middle of the anchor rod and considerable plastic deformation at the end. The insufficient preload could lead to ineffective control of surrounding rock deformation and poor effectiveness when supporting weak coal seams. Meanwhile, when the preload is too large, the surrounding rock deformation is insufficient and the stress on the rod is large, resulting in local stress concentration and breakage of anchor rod or nut loosening.

Figure 4 shows the stress cloud map of the anchor rod under load, with the gray rod representing the initial state, and includes strain–displacement evolution curves at the anchor rod end. In the initial deformation stage, the stress on the anchor rod is less than the yield limit, leading to the lower deformation rate and amount.

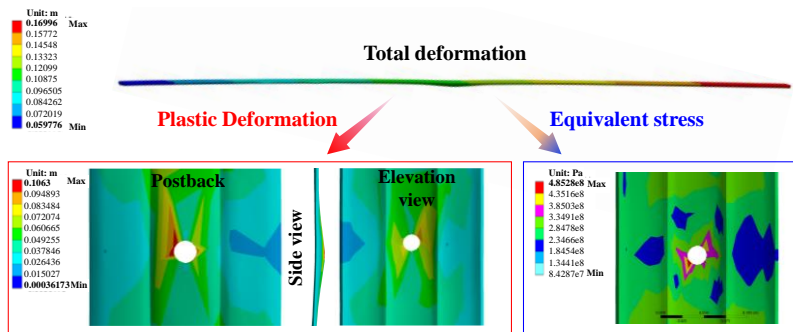


Fig. 4. Results of steel strip damage

When the stress on the anchor rod approaches the yield limit, the rod enters the yield strengthening stage, and the deformation increases continuously with the stress increasing. Meanwhile, the deformation rate increases sharply and the rod gradually yields when the stress reaches 426 MPa. In addition, the significant tensile deformation occurs at the anchor rod end under the combined action of the surrounding rock deformation and preloading force. At the same time, the subsidence of the upper surrounding rock causes the shear failure at the anchor rod end. Ultimately, the anchor rod fractures under the combined action of tension and shear force (Wu et al. 2013).

### 3.1.3. THE STEEL STRIP FAILURE MODE

The W-shaped steel strip is selected as the main supporting component. Figure 5 shows the deformation characteristics of the steel strip, where the deformation in the middle of the steel strip is relatively small, with the decrease of 0.12 m. On the contrary, the two ends are bent upwards due to the surrounding rock deformation, with a maximum deformation of 0.17 m. When the surrounding rock occurs significant deformation,

the connection between the steel strip and the edge of the pallet is prone to upward bending. At the same time, constrained by the pallet, the composed action of compression and shear on the steel strip increases. Therefore, the steel strip is prone to plastic deformation and stress concentration, which leads to compression failure (Meng et al. 2018; Yang et al. 2022).

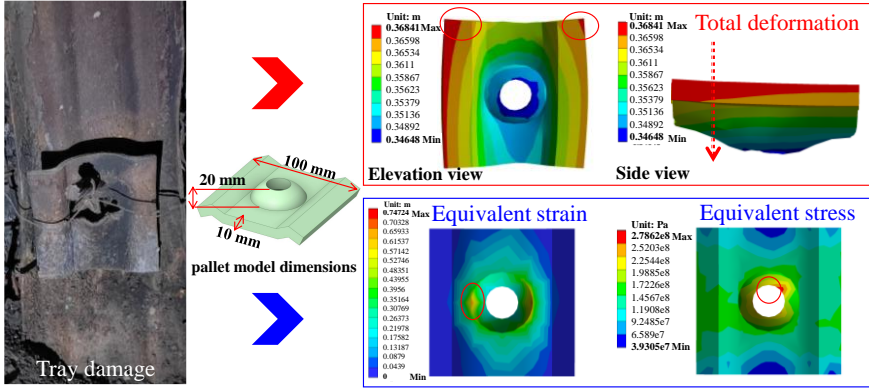


Fig. 5. Results of pallet deformation

### 3.1.4. THE PALLET FAILURE MODES

This section analyzes the failure characteristics of mining discotic pallets under the surrounding rock deformation. The pallet material is Q235 steel, with dimensions of  $100 \times 100 \times 10$  mm and arch height of 20 mm, and the model is shown in Fig. 6.

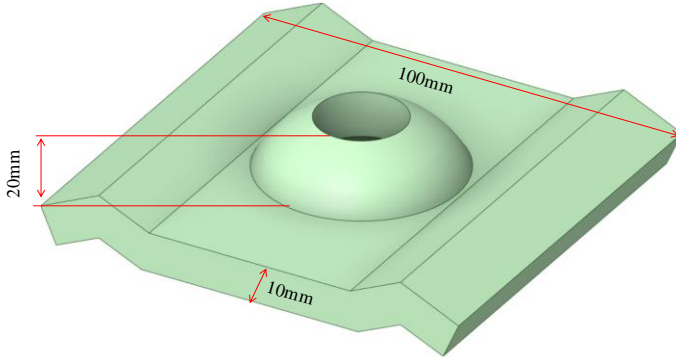


Fig. 6. Schematic diagram of pallet model dimensions

It can be seen from the red part circled in Fig. 7 that the deformation of the two shoulder angles of the pallet is the largest and asymmetrical. The opening deformation of the pallet is 0.24 m, the edge deformation is 0.30 m, and the opening subsidence is

40 mm, which has a concave feature. The equivalent force cloud map shows that the pallet is in the unidirectional stress state. Due to the nut constraint, stress concentration occurs in the hole, as shown in the red circle of the stress cloud diagram in Fig. 7, and the maximum stress is 278 MPa. In addition, the pallet bottom generates vertical displacement due to the surrounding rock deformation, while the pallet arch sinks under the preload action, so the pallet would fail when the edges of the two components are at the same level. In summary, because of the poor stress dispersion ability in the arch area, the uneven stress distribution of the pallet, and under the action of compression, bending, and torsion, the stress constantly accumulating leads to the pallet deformation and damage ultimately (Pan et al. 2023).

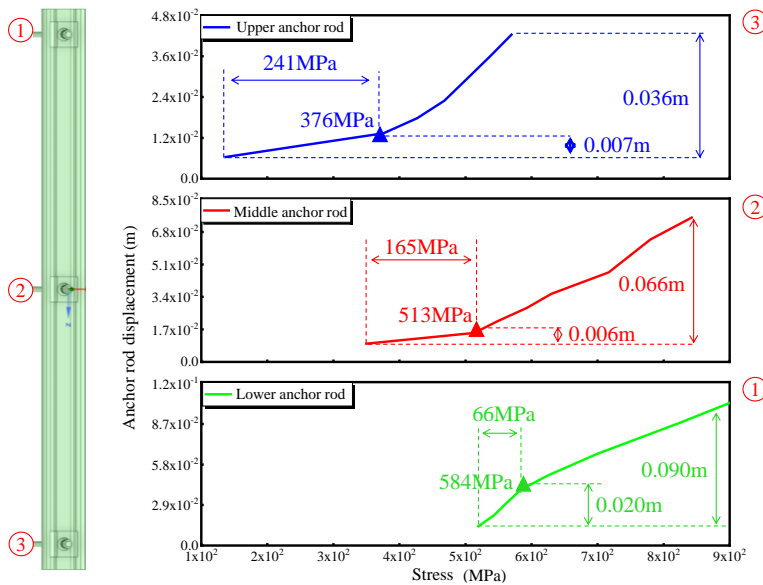


Fig. 7. Results of pallet deformation

### 3.2. THE MULTIPLE ANCHOR SUPPORT

When multiple anchor rods are used for support, each component is connected by steel strips. The supporting structure and the deformation of surrounding rock are under pressure together, and the deformation of surrounding rock is controlled from point to surface. To further investigate the local failure characteristics of anchor rod under the surrounding rock deformation, a single-row anchor rod support model is established based on the numerical model of a single anchor rod. Figure 8 shows that the anchor rod spacing is 1000 mm.

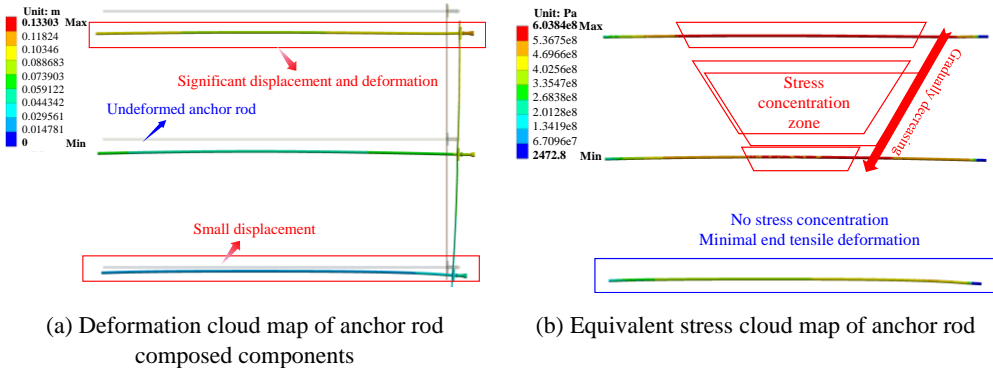


Fig. 8. Deformation results of anchor rod combination unit

### 3.2.1. THE FAILURE MODE OF ANCHOR ROD-NUT

Figure 9 shows the stress–strain curves of the anchor rod. The anchor rods deformation is mainly divided into two stages. In the initial stage, the deformation rate of the anchor rod is relatively low, at this time, the stress applied on the rod is lower than its yield strength. In the yield strengthening stage, the deformation rate gradually increases, and the rod would break when the stress on the anchor rod exceeds the yield strength. The stress at the point of sudden increase in deformation rate of the upper anchor rod in the surrounding rock is 584 MPa, which in the middle anchor rod is 513 MPa, and the lower anchor rod is 376 MPa. In addition, the initial deformation rate of the upper anchor rod in the surrounding rock is  $3.0 \times 10^{-4}$  m/MPa, the middle anchor rod is  $3.6 \times 10^{-5}$  m/MPa and the lower anchor rod is  $2.9 \times 10^{-5}$  m/MPa. The results indicate that the initial deformation rate and the stress at the inflection point of the deformation rate of the upper anchor rod are the highest when the rod is distributed longitudinally along the surrounding rock.

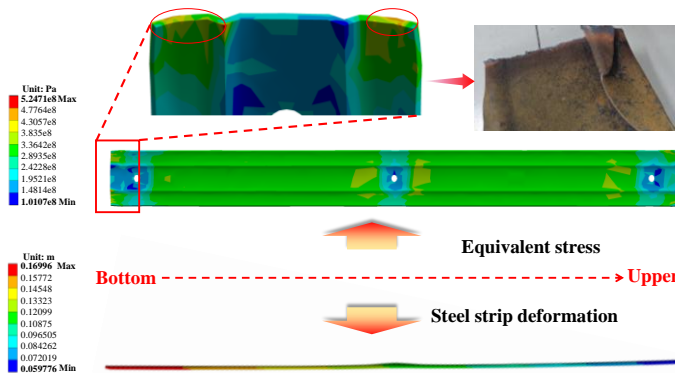


Fig. 9. Results of steel strip damage

Table 2 shows that the relative displacement between the nut and the anchor rod of 0.0117~0.0118 m is greater than the initial distance. The stress on the nut end gradually increases with the surrounding rock deforming, and the nut falls off when the nut bearing force exceeds the frictional force provided by the thread. The similar displacements of the three nuts indicate that the reason for the nut falling is only related to its bearing frictional and preload force, instead of the degree of the surrounding rock deformation.

Table 2. Relative displacement of nuts at different positions

Upper nut of steel strip [m × 10 <sup>-4</sup> ]	Middle nut of steel strip [m × 10 <sup>-4</sup> ]	Lower nut of steel strip [m × 10 <sup>-4</sup> ]
5.19	5.19	5.16
21.88	21.88	21.87
39.54	39.56	39.40
60.10	60.12	60.02
80.64	80.66	80.46
97.90	97.83	97.56
108.29	108.21	107.88
118.67	118.52	117.95

Figure 10 shows the deformation of the combined anchor rod unit. Figure 10a shows that the deformation of the anchor rods decreases from top to bottom, among which the deformation of the upper anchor rod is the largest and the deformation of the lower anchor rod is the smallest. Figure 10b shows that the middle part of the upper and middle anchor rods has a large range of stress concentration, while the lower anchor rod has no stress concentration as a whole. Combined with the deformation and stress distribution of the combined anchor rod, it can be seen that the deformation of the surrounding rock occurs from top to bottom, resulting in the decrease of the deformation of the anchor rod from top to bottom. At the same time, the upper and middle anchor rods bear most of the stress generated by the deformation of the surrounding rock, and the stress concentrates at the end of the anchor rod, resulting in a smaller stress at the end of the lower anchor rod. Under the support of the combined anchor rods, the deformation of the surrounding rock is effectively controlled compared with the single anchor rod, and the overall instability will not occur.

As Figure 11 shows that the nut occurs strain response from bottom to top in sequence (Si et al. 2023). In addition, the strain of nut decreases sharply at the same time, which is because the nuts bearing force gradually spreads to other components with the degree of rock deformation increasing under the influence of preload force, resulting the strain of nuts decreasing in a short time. But as the degree of the surrounding rock deformation increases, the force generated by the surrounding rock and the preload are re-concentrated in the nut, so the strain curves of the nuts show a trend of increasing first then decreasing.

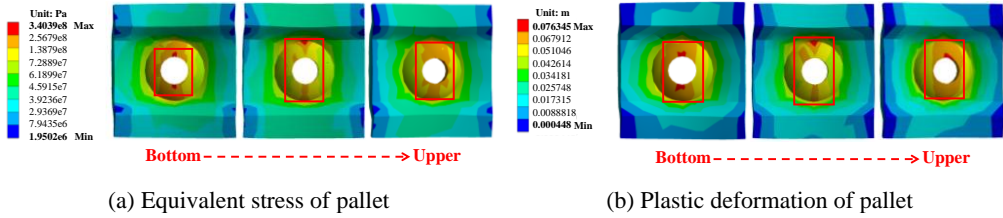


Fig. 10. Results of pallet damage

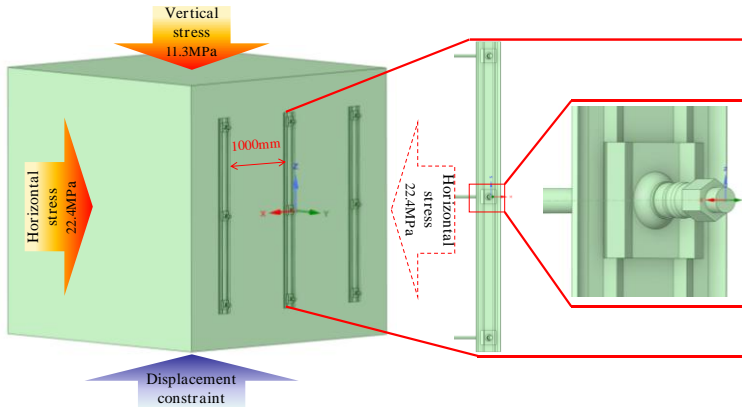


Fig. 11. Numerical model of multiple row anchor rod support

3.2.2. THE STEEL STRIP FAILURE MODES

Figure 12 shows the deformation characteristics of the steel strip. The steel strip exhibits the significant stress concentration at the sharp corners of the end, with the maximum stress of 524 MPa. On the contrary, the stress distribution of the steel strip without anchor rods is uniform, with a stress value of 300 MPa, indicating that the anchor rods control the surrounding rock deformation. The stress concentration of the steel strip under multiple anchor rods occurs at the sharp corners of the end, which is because the number of anchor rods increasing effectively disperses the stress generated by surrounding rock deformation and reduces the local deformation of the surrounding rock. When using single anchor rod support, the surrounding rock deformation is only constrained at one point, so the effect of the surrounding rock deformation accumulates continuously in single area, ultimately leading to significant stress concentration. The deformation of the steel strip at the anchor support is relatively small, while the steel strip without anchor support induces bending deformation, so the deformation trend shows a wave shape. Due to the fragility of the steel strip without anchor support, the recombination action of compression and shear at the junction with the edge of the pallet increases with the surrounding rock deformation, leading to the compression failure of the steel strip (Wu et al. 2013).

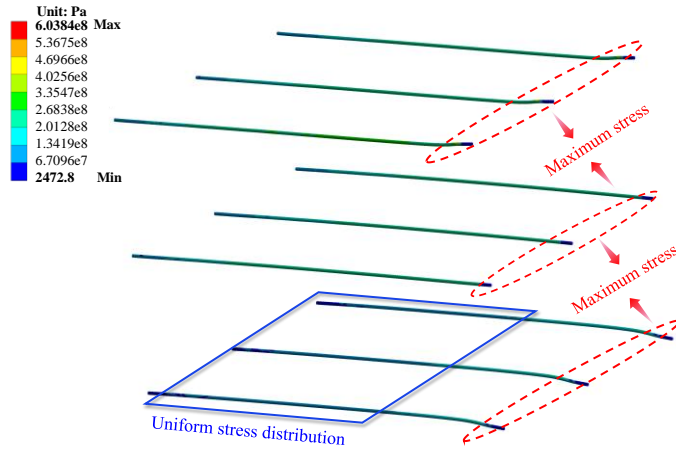


Fig. 12. Equivalent stress cloud map of anchor rods

3.2.3. THE PALLETS FAILURE MODES

Figure 13 shows the pallet deformation characteristics, Fig. 13a is the equivalent stress cloud map and Fig. 13b is the plastic deformation cloud map. The pallet bottom is bent upwards due to the surrounding rock deformation. On the contrary, the hole opening is depressed downwards because of the suppression effect of the nut, so the pallet shows a deformation trend of arch depression and surrounding uplift. In addition, the middle pallet shows significant axial displacement, while the two end pallets experience tilting deformation.

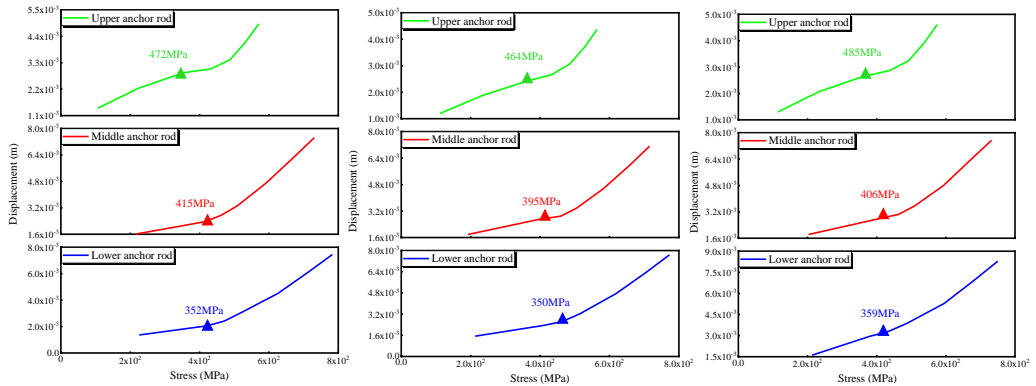


Fig. 13. Results of pallet damage

The failure characteristics of a single anchor rod indicate that there is a significant stress concentration phenomenon at the hole opening of the pallet, and the concentration range gradually decreases from top to bottom of surrounding rock, with the maximum

stress reaching 340 MPa. The pallet opening is prone to plastic deformation because the pallet arch is the main area bearing force. When the preload is large, the pallet could not disperse the stress of the surrounding rock. Therefore, the hole opening gradually occurs stress concentration. At the same time, the upper part of the surrounding rock deforms first, which leads to the obvious stress concentration and plastic deformation of the pallet in the upper part of the surrounding rock (Pan et al. 2023).

When the multiple anchor rods are used for support, the failure characteristics of the pallet are different from those of a single anchor rod. The support structure only controls the surrounding rock deformation from a single point with the single anchor rod, resulting in the force generated by surrounding rock deformation being greater than the restraining effect of the preload force. Therefore, the pallet has significant plastic deformation at the bottom. However, the multiple support structure could reduce the surrounding rock deformation. At the same time, the pallet is subjected to unidirectional force, and high preloading force causes significant stress concentration and plastic deformation characteristics on the hole opening. In summary, the main reason for the pallet damage is the poor stress dispersion ability of the pallet arch. When the pallet is subjected to high stress, the stress could not be diffused to the bottom, ultimately leading to uneven stress distribution and local stress concentration.

### 3.3. THE COMBINED ANCHOR ROD SUPPORT

In order to investigate the surrounding rock deformation characteristics under multiple-row anchor rod support and the differences in failure causes of various components under different simulation conditions, a new support structure is added on both sides of the original steel strip based on the multi-row anchor rod model. The steel strip spacing is 1000 mm. The size and parameters of the newly added composed anchor rods are the same as those of the original model. Figure 14 shows the analysis unit model of composed anchor rods.

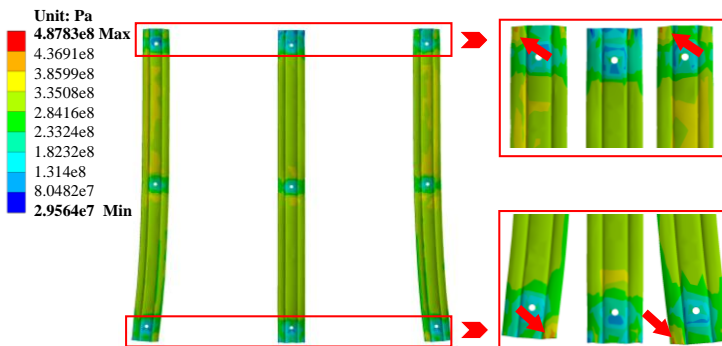


Fig. 14. Equivalent stress cloud map of steel strip

## 3.3.1. THE FAILURE MODE OF ANCHOR ROD NUT

Figure 15 shows the stress-strain curves of the anchor rod. When the anchor rod is distributed longitudinally along the surrounding rock, the stress and deformation rate gradually decrease as the support position moves downward, and the inflection point of the deformation rate also gradually decreases. In addition, the deformation phenomenon is caused by the surrounding rock deformation under the complex action of vertical and horizontal stresses, which presents higher stress and greater deformation for the middle anchor rod than the side anchor rod. The deformation rate of the anchor rod increases sharply near the yield strength. Meanwhile, the point where the deformation rate of the anchor rod changes in the upper part of the surrounding rock experiences the highest stress. When the surrounding rock has initial deformation, the stress on the anchor rod is lower than the yield strength, resulting in smaller stress and lower deformation rate. On the contrary, when the stress on the anchor rod approaches the yield strength, the deformation rate of the rod increases sharply until breaks.

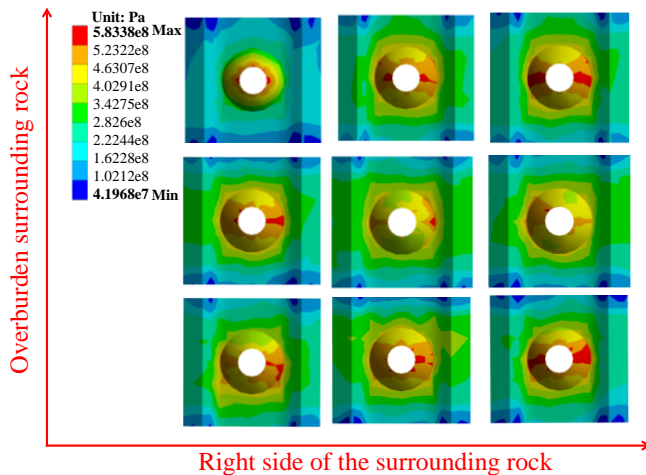


Fig. 15. Equivalent stress cloud map of pallet

Figure 16 shows the equivalent stress cloud map of the anchor rod. Different from the simulation results of multiple anchor rods, the maximum stress of the anchor rod occurs at the end, and the stress on both sides of the rod is the smallest. The maximum stress of the anchor rod reaches 600 MPa, which exceeds the yield strength of the rod. Therefore, the rod is prone to shear fracture. After the tunnel excavating, the stress of the surrounding rock is transferred from the outside to the inside, and the upper surrounding rock experiences bending deformation at the same time.

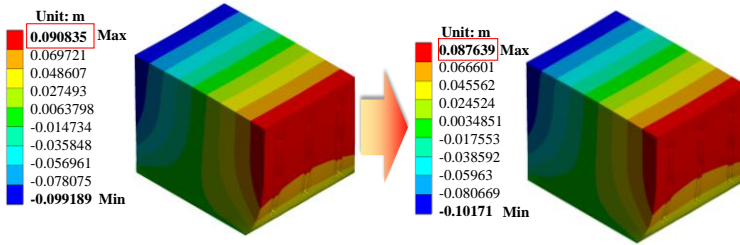


Fig. 16. Comparison of surrounding rock deformation

Table 3. Relative displacement between nuts and anchor rods

Left side nut of surrounding rock [m]			Middle nut of surrounding rock [m]			Right side nut of surrounding rock [m]		
Upper	Middle	Blow	Upper	Middle	Blow	Upper	Middle	Blow
0.001	0.001	0.001	0.002	0.001	0.001	0.002	0.001	0.000
0.003	0.003	0.002	0.003	0.003	0.002	0.003	0.003	0.002
0.007	0.006	0.003	0.007	0.006	0.003	0.006	0.006	0.003
0.012	0.011	0.006	0.012	0.011	0.006	0.012	0.011	0.005
0.024	0.020	0.011	0.024	0.020	0.010	0.023	0.021	0.011
0.034	0.030	0.016	0.034	0.028	0.015	0.034	0.030	0.016
0.043	0.037	0.020	0.042	0.036	0.019	0.042	0.038	0.021

Table 3 shows the nuts relative displacement. The maximum displacement of the nut reaches 0.04 m, indicating that the nut falls off. As the support position moves downward, the nut displacement gradually decreases. The change trend of nuts in each row is the same, which is consistent with the deformation law of nuts under multi-anchor support. When nuts horizontally distribute along the surrounding rock, the displacement of the nuts on both sides of the rock are the same and greater than that of the middle nut. The above research results show that the tensile stress generated by the compression of the surrounding rock is transmitted to the nut through the steel strip and the pallet. Then, when the effect of the surrounding rock deformation is greater than the frictional force provided by the thread, the nut gradually shifts outward until it completely falls down from the anchor rod.

3.3.2. THE STEEL STRIP FAILURE MODE

Figure 17 shows the deformation of the steel strip. The deformation trend and characteristics are the same as those under multi-anchor support, namely wavy. There is significant deformation at the upper end of the steel strip. The deformation of the upper part of the surrounding rock is not effectively controlled, resulting in the steel strip bending. Because the surrounding rock on both sides is first affected by horizontal

stress, the deformation of surrounding rock on both sides is greater than that in the middle, resulting in relatively large deformation of steel strips on both sides.

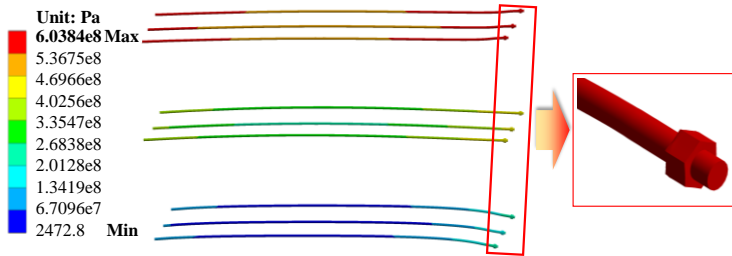


Fig. 17. Deformation results of steel strip

Figure 18 shows the equivalent stress cloud map of the steel strip. The stress distribution of the steel strip is uniform, and the stress concentration and maximum plastic deformation occur at the sharp corners, which is similar to the deformation characteristics of the steel strip under multi anchor support. The simulation test results of the single anchor rod and the single-row anchor rods, which could be concluded that when the surrounding rock deformation is large, the stress concentration phenomenon in the steel strip is caused by the high preload force. In addition, the surrounding rock deformation leads to the steel strip experiencing greater stress and bending upwards under the preload force. The composed action of compression and shear at the junction of the steel strip and the pallet edge is enhanced, inducing the compression failure of the steel strip.

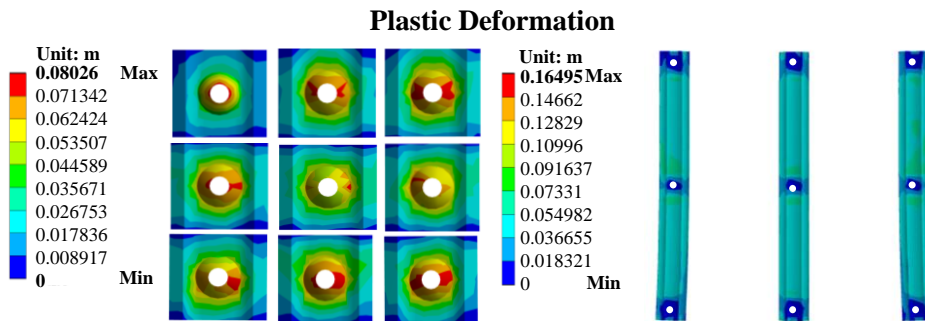


Fig. 18. Equivalent stress cloud map of steel strip

### 3.3.3. THE PALLET FAILURE MODES

Figure 19 shows the equivalent stress cloud map of the pallet. The maximum equivalent stress of the pallet occurs at the hole opening and gradually spreads circularly along the hole diameter, so the equivalent stress of the upper pallet of the surrounding rock is

high. Due to the large preload force and insufficient surrounding rock deformation, the pallet arch is only subjected to unidirectional force, and the stress at the circular arch could not diffuse, resulting in significant stress concentration at the orifice ultimately. In addition, the lower surrounding rock deformation is relatively small under the vertical stress, resulting in lower stress on the lower pallet. After the three sides are compressed, the upper and two sides of the surrounding rock deform first, and the stress gradually spreads to the middle of the surrounding rock with the deformation increasing. In addition, the stress on the middle pallet is less than the stress on both sides of the pallet.

Figure 20 shows the plastic deformation cloud map of the pallet. The plastic deformation of the pallet occurs at the orifice, and the upper part of the surrounding rock has a larger plastic deformation, while the middle part has the smallest deformation. Meanwhile, the deformation trend is consistent with that of the equivalent stress. The equivalent stress analysis results show that there is no significant deformation of the supporting components in the middle of the surrounding rock. Additionally, the pallet is bent upwards due to the surrounding rock deformation, but the arch area of the pallet occurs concave deformation because of the preload force. When the arch of the pallet is deformed and aligned with the surrounding edges, the pallet structure is completely destroyed. The above results indicate that the arches of the pallets are the main yielding area, so the surrounding rock pressure and preload force first act on the arches of the pallets and then gradually spread to the edge, and the deformation in the middle of the pallet is larger.

Fig. 19. Equivalent stress cloud map of pallet

Fig. 20. Plastic deformation cloud map of pallet

## 4. OPTIMIZATION DESIGN OF COMPOSED ANCHOR ROD SUPPORT

### 4.1. THE FAILURE MECHANISM OF COMPOSED ANCHOR RODS

By analyzing the characteristics of single point failure and local failure of composed anchor rods, which concludes that the upper part of the surrounding rock first experiences stress and has significant subsidence deformation, while the middle part of the surrounding rock experiences lower stress. Therefore, the failure of composed anchor components occurs in the upper area of the surrounding rock, and the deformation is relatively large. The failure characteristics of nuts are different from those of other supporting components. The deformation of nuts does not change with different the supporting positions, indicating that the reason for nut loosening might only be related to

the frictional force and preload force provided by the thread, rather than the supporting position and the degree of surrounding rock deformation (Zhao et al. 2023). Because of the combined action of preload and surrounding rock deformation, the stress concentration and plastic deformation characteristics at the hole opening are significant. Moreover, the stress on the pallet hole opening gradually spreads outward with the deformation increasing. The lower edge of the pallet bends upward after being subjected to force, and the circular arch area is gradually flattened by the preload suppression effect. When these two deformed states are at the same level, the pallet fails and breaks. Due to the deformation of the surrounding rock and the restraining effect of the pallet, the middle of the steel strip is concave and the edge is bent upward. In addition, the compression-shear composed action at the connection between the steel strip and the pallet edge is enhanced, so the steel strip is prone to compression failure.

#### 4.2. THE OPTIMIZATION OF SUPPORT MEASURES

The following support optimization measures are proposed for the different failure mechanisms of the mentioned combination anchor.

(1) The preload force exerted by the anchor rod on the surrounding rock is adjusted from 100 to 80 kN. The main reason for nut detachment is the excessive preload force. Under the action of preload force, the axial displacement of the supporting structure is limited. The nut would loosen or detach from the anchor rod when the stress on the nut is greater than the frictional force generated by the thread. Therefore, the preload force should be appropriately reduced in practical engineering.

(2) The radius and height of the pallet arch are increased by 5 mm. Meanwhile, the dimensions of the lower part of the pallet and the width of the steel strip are expanded by 50 mm. The arched area of the pallet could effectively disperse the stress. The existing studies show that increasing the radius and height of the pallet arch area could effectively improve the pressure bearing effect (Fu et al. 2021; Yan et al. 2023).

(3) As the surrounding rock in different regions is subjected to different stresses, there are variations in the degree of the surrounding rock deformation. Therefore, the preload force of the anchor rod should be adjusted appropriately according to different support positions.

#### 4.3. OPTIMIZATION RESULTS ANALYSIS

(1) Figure 21 shows the comparison of surrounding rock deformation. When the preload force on the anchor rod is adjusted from 100 to 80 kN, the lateral deformation of the surrounding rock decreases from 0.09 to 0.08 m. The above phenomenon indicates that when the preload force is high, the combined anchor rod could not achieve the optimal support effect. By reducing the preload force of anchor rods on the surround-

ing rock could effectively control the surrounding rock deformation and reduce the failure rate of supporting components.

(2) As shown in Fig. 22, the stress in the middle of the anchor rod is relatively high, and the lateral deformation at the end of anchor are significant, with the elongation rate of 6%. The regulations stipulate that the elongation rate of the anchor rod should be greater than 5%, and the elongation rate of Q500 steel should be less than 7%. After reducing the pretension, the anchor rod has tensile deformation, but the lateral deformation is within the bearing range without a breaking phenomenon. In addition, the nut does not detach from the anchor rod and the displacement decreasing. In summary, the proposed optimization measures effectively control the surrounding rock deformation as well as the failure rates of anchor rods and nuts.

Fig. 21. Comparison of surrounding rock deformation

Fig. 22. Equivalent stress cloud map of anchor rods

(3) Scholars propose that the arch of the pallet is the main part that bears and the disperses stress. The increase of the bottom area and the height of pallet arch could reduce the stress concentration and failure rates (Liu et al. 2023). The experimental results are shown in Figs. 23 and 24.

(a) Equivalent force cloud map (b) Plastic Deformation

Fig. 23. Cloud map of pallet deformation

After increasing the pallet size, the force on the pallet hole is evenly distributed and spreads in a regular manner. There is no significant stress concentration at the pallet bottom, and no obvious plastic deformation occurs at the hole opening either. Similarly, after increasing the width of the steel strip, there is no plastic deformation at the sharp corners of edges. Moreover, there is no stress concentration at the connection between the steel strip and the edge of the pallet. The above research results indicate that the proposed support optimization measures effectively reduce the failure and damage of the pallet and steel strip.

(a) Equivalent force cloud map (b) Plastic Deformation

Fig. 24. Cloud map of steel strip deformation

In summary, increasing the pallet size and steel strip could reduce the occurrence of plastic deformation at the pallet opening and suppress the damage of the steel strip and pallet. In addition, reducing the preload force of anchor rods could effectively control the surrounding rock deformation and reduce the stress concentration of the rod and nut as well as plastic deformation.

## 5. CONCLUSIONS

In this paper, the mechanical calculations and numerical simulation were used to study the single point and local failure characteristics of composed anchor in gob-side entries. The corresponding support optimization measures were proposed. The specific conclusions are as follows.

(1) The deformation rate of the anchor rod gradually rises with the surrounding rock deformation increasing. In addition, as the support position of the rod moves downward, the turning point of the rod entering the yield strengthening stage decreases. Because the upper part of the surrounding rock is the first to be subjected to the stress and deformation, the supporting components experience plastic deformation. In addition, the stress concentration and plastic deformation of the supporting components in the middle of the surrounding rock are relatively small.

(2) The main reason for the nut invalidity is that the stress on the nut exceeds the frictional force provided by the thread. Moreover, the deformation of the anchor rod at different support positions is identical, indicating that the detachment of the nut is solely related to the frictional force and preload force provided by the thread, rather than the degree of deformation of the surrounding rock or the position of anchor rod support.

(3) The arch of the pallet is the main load-bearing part and the stress transmitting downward through the arch. When the edge of the pallet is at the same level as the arched edge, the pallet is damaged. Under the surrounding rock deformation, the steel strip produces a combined compression-shear action at the junction with the edge of the pallet, and this effect gradually increases with the surrounding rock deformation increasing, ultimately leading to the steel strip damage.

(4) Under the support optimization measures that could reduce pretension force and increase pallet and steel strip size, the surrounding rock deformation is reduced by 0.01 m, and the lateral deformation of the anchor rod and nut is also reduced. Moreover, there is no obvious stress concentration at the joint between the steel strip and the pallet or at the holes of the steel strip and the pallet. Finally, the above phenomenon indicates that the proposed measures effectively control the surrounding rock deformation as well as the failure rate of composed anchor rods.

## ACKNOWLEDGEMENTS

This study was supported by the National Natural Science Foundation of China (52404132), the Taishan Scholars Project Special Fund (tsqn202312195) and the Youth Innovation Team Development Plan of Colleges and Universities of Shandong Province (2022KJ320).

## DECLARATIONS

The authors declare that they have no conflict of interest existing in the submission of this manuscript.

## REFERENCE

- [1] LUBRYKA D., MADZIARZ M., 2023, *Underground testing of load bearing capacity of rock bolting as part of the verification of its proper selection*, Mining Science, 30, 63–81.
- [2] JING H, SU H, MENG B, et.al., 2022, *Field test research on anchorage mechanical characteristics of roadway bolt*, Journal of China University of Mining and Technology, 51(1): 16-23.
- [3] ZHANG R.J., ZHENG J.J., LI P.Y. et al., 2012, *A method for predicting mechanical behaviour of HPJG-Anchors*. Part I: *Mechanical characteristics and load transfer models*, Computers and Geotechnics, 45: 62-73.
- [4] SHI X.D., BAI J.W., FENG G.R. et al., 2024, *Mechanical response of coal pillar-backfill composite confined by CFRP jackets: parametrical study*, Construction and Building Materials, 443, 14.
- [5] WU G.S., YU W.J., PAN B. et al., 2025, *Failure mechanics mechanisms and permeability stage evolution of limestone considering wave velocity and failure surface characteristics*, Soils and Foundations, 65 (1), 22.
- [6] WANG K., BAI J.W., FENG G.R., 2025, *Measurement of impact failure evolution of coal samples under in-situ water pressure environment: Visualization SHPB experiment and damage model analysis*, Measurement, 253, 15.
- [7] ZEQRİ K., IBİSHI G., SHABANI M. et al., 2021, *Preliminary support design for underground mine adit, Artana mine, Kosovo*, Mining Science, 28, 141–159.
- [8] SAKHNO I., KORZENIOWSKI W., SHEPTAK K. et al., 2021, *Influence of adhesion on stress–strain condition alongside of a full column resin cartridge rock bolt*, Mining Science, 28, 233–245.
- [9] BONDARENKO V., KOVALEVSKA I., SYMANOVYCH G. et al., 2018, *Geomechanics of interference between the operation modes of mine working support elements at their loading*, Mining Science, 25, 219–235.
- [10] MING W., YANG X., PAN Y. et al., 2023, *Field test and numerical simulation of initial support effect of negative Poisson's ratio anchor cable under strong impact and vibration*, Tunnelling and Underground Space Technology, 133, 104955.
- [11] MESUTOGLU M., OZKAN I., 2024, *Evaluation and comparison of rock bolting versus steel arch support systems in thick coal seam underground galleries: a case study*, Mining Metallurgy and Exploration, 41, 1719–1737.
- [12] CAO J., ZHANG N., WANG S. et al., 2020, *Physical model test study on support of super pre-stressed anchor in the mining engineering*, Engineering Failure Analysis, 118, 104833.
- [13] ZHOU J., JIE Z., DONG H. et.al., 2023, *Pallet bolt in Liangjia coal mine simulation study on supporting performance of iron-wood composed*, Coal Technology, 42 (8), 65–70.
- [14] LIU Y., XIA C., WU F. et.al., 2020, *A combined support technology of long and short bolts of soft rock tunnels under high ground stresses*, Chinese Journal of Rock Mechanics and Engineering, 39 (1), 105–114.

- [15] KHADEMIAN Z, SEARS M., 2024, *Contribution of individual support components to roof stability in a longwall gate road*, Mining Metallurgy and Exploration, 41(2): 695-705.
- [16] WANG D, HE M, TAO Z, et al., 2023, *Effects of high prestress and rock loading rate on deformation behaviors of high strength and high-toughness steel for rock bolts*, Chinese Journal of Rock Mechanics and Engineering, 42(9): 2212-2223.
- [17] TAN Y, MA Q, ZHAO Z, et al., 2019, *Cooperative bearing behaviors of roadside support and surrounding rocks along gob-side*, Geomechanics and Engineering, 18(4): 439-448.
- [18] XIE S, LI H, CHEN D, et al., 2024, *Research on the control technology and key parameters of external anchor-internal unloading of surrounding rock during gob-side entry driving under severe mining of 1000-m-deep mine*, Rock Mechanics and Rock Engineering, 57(4): 2913-2932.
- [19] WANG Q, PAN R, LI S, et al., 2018 *The control effect of surrounding rock with different combinations of the bolt anchoring lengths and pre-tightening forces in underground engineering*, Environmental Earth Sciences, 77(13): 501.
- [20] ZHAO H, SU H, QIN X, et al., 2023, *Experiment and numerical simulation of strength and stress distribution behaviors of anchored rock mass in a roadway*, Geofluids, 2023: 9311206.
- [21] ZHA W, WU D., 2018, *Study on coupling relationship between surrounding rock deformation and support parameters in deep roadway*, International Conference on Civil, Architecture and Disaster Prevention, 218: 012118.
- [22] ZHANG J, LIU L, LIU C, et al., 2022, *Mechanism and application of new prestressed yield bolt for controlling deep high-stress rock mass*, Tunnelling and Underground Space Technology, 119: 104254.
- [23] RONG H, PAN L, LI X, et al., 2021, *Analysis on influence factors of roadway instability in high-stress, steeply inclined extra-thick coal seam*. Advances In Civil Engineering 2021: 4676685.
- [24] WU X, ZHANG Y, ZHANG Z, et al., 2019, *Influence of radial stiffness of surrounding rock on dynamic behavior of end-anchored rock bolt under impact loading*, Latin American Journal of Solids and Structures, 21(9): e564.
- [25] SI L, LOU J, YANG J, et al., 2022, *Deformation and stress characteristics of anchor bolt under axial impact*, Journal of China Coal Society, 47(10): 3645-3653.
- [26] KANG H, LIN J, WU Y, et al., 2015, *Mechanical performances and compatibility of rock bolt components*, Journal of China Coal Society, 40(1): 11-23.
- [27] LIU J, SUN H, ZHANG Z, et al., 2019, *Research on macro-mechanics mechanism of bolt fracturing and its control with high pre-tensioned force*, Coal Science and Technology, 47(1): 91-96.
- [28] PAN L, ZHAO T, XING M, et al., 2023, *Research on compression deformation process and load-bearing characteristics of saucer pallet used in mining*, Journal of Shandong University of Science and Technology (Natural Science), 42(2): 53-61.
- [29] WU G S, YU W J, ZUO J P, et al., 2020, *Experimental and theoretical investigation on mechanisms performance of the rock-coal-bolt (RCB) composite system*, International Journal of Mining Science and Technology, 30(6): 759-68.
- [30] WU G S, YU W J, ZUO J P, et al., 2020, *Experimental investigation on rockburst behavior of the rock-coal-bolt specimen under different stress conditions*, Scientific Reports, 10(1): 17.
- [31] WU Y, KANG H., 2013, *Failure mechanism study on tail of high strength bolt*, Journal of China Coal Society, 38(9): 1537-1541.
- [32] MENG X R, PENG R, ZHAO G M, et al., 2018, *Roadway Engineering Mechanical Properties and Roadway Structural Instability Mechanisms in Deep Wells*, Ksce Journal of Civil Engineering, 22(5): 1954-66.
- [33] YANG Y, CHEN X, XUE Y C, et al., 2022, *Experimental investigation on shear performance of reinforced concrete beams retrofitted by pre-stressed steel strips*, Structures, 43: 767-78.
- [34] FU Y., 2021, *Numerical simulation study on the bending mechanical properties of W-shaped steel*

- strip*, Technology and Market, 28(10): 119-120.
- [35] ZHAO Y, ZHANG N, ZHENG X., 2016, *Experimental study of axial stress distribution and transfer along the bolt rods in an underground coal mine*, Arabian Journal of Geosciences, 9(1): 30.
- [36] YAN R, NING J, ZHANG Z, et al., 2023, *Analysis of diffusion effect and influencing factors of anchoring force of arched rock bolt support plate*, Safety in Coal Mines, 54(4): 126-131.
- [37] LIU X, WU Y, TAN Y, et.al., 2023, *Breaking mechanism of inclined bolts in deep mine roadway with high horizontal stress and the timing of strengthening support*, Journal of China Coal Society, 48(2): 609-622.